Waste Management 208 (2025) 115141

Contents lists available at ScienceDirect

Waste Management

journal homepage: www.elsevier.com/locate/wasman

Research Paper

Fabrication of new glass–ceramic materials from float glass and slag waste by modulation of the cooling rate

Paola Stabile [a,*], Francesco Vetere [b], Letizia Giuliani [c], Cristina Siligardi [d], Consuelo Mugoni [d], Manuela Nazzari [e], Gianluca Iezzi [c,e,f]

[a] Scuola di Scienze e Tecnologie, sez. di Geologia, Universita' di Camerino, Via Gentile III da Varano, 7, 62032 Camerino, Italy
[b] Dipartimento di Scienze Fisiche, della Terra e dell'Ambiente (DSTA), University of Siena, Via Laterina, 8, 53100 Siena, Italy
[c] Dipartimento di Ingegneria & Geologia (InGeO), Università G. D'Annunzio di Chieti-Pescara, Via dei Vestini 31, 66100 Chieti, Italy
[d] Dipartimento di Ingegneria "Enzo Ferrari", Università di Modena e Reggio Emilia, Via Pietro Vivarelli, 10, 41125 Modena, Italy
[e] Istituto Nazionale di Geofisica e Vulcanologia, INGV, Via di Vigna Murata, 605, Roma, Italy
[f] UdA-TechLab, Centro di Ricerca, Università G. D'Annunzio di Chieti-Pescara, Via dei Vestini 31, 66100 Chieti, Italy

ARTICLE INFO

Keywords:
Glass waste
Copper slag
Secondary raw materials
Melting
Solidification
Cooling rate
Glass-ceramics

ABSTRACT

This study explores an alternative route to recycle waste materials from float glass (FG, 30 wt%) and copper slag (CS, 70 wt%). The FG is a silica-rich glass, while the CS is rich in Fe and Zn. They were melted at 1550 °C to obtain a homogeneous glass that was then re-melted and cooled at 10 (low) and 500 (high) °C/h to produce a glass–ceramic. X-Ray Powder Diffraction, Scanning Electron Microscope and Electron microprobe characterisations show that both products contain spinel crystals within an abundant glassy matrix. At 500 °C/h, unexpectedly, the glass–ceramic contains a higher content (30.0 ± 5.5 area%) of tiny and long dendrites (spinifex) of spinels than at 10 °C/h (13.7 ± 2.2 area%); at the low rate, spinels are skeletal (large crystals) to dendritic (tiny and short) and larger than at high rate. This unveils that the estimated crystal growth rate (10^{-7} cm/s) is higher at 500 °C/h. The crystal-chemistry of spinels results in more enriched Fe and Zn at 10 °C/h than at the high rate. This approach is promising for various applications or for concentrating valuable transition metals (Fe, Zn) as a function of cooling rate and type and quantity of starting waste materials; also, it avoids treatments with additives or fluxing agents and it provides, thanks to the dielectric properties shown, a strong potential for industrial use as a microwave absorber.

1. Introduction

Waste management is increasingly relevant and complex, especially in developed countries. Solid waste materials mainly originate from construction, metallurgical, mining and energy-producing sectors (Dino et al, 2020; Kurtulus et al., 2021; Spooren et al., 2020; Zibret et al., 2020). Several wastes can also accumulate in nature, prompting environmental pollution (Coetzee et al., 2020; Ramteke et al., 2021). For instance, the (legal or illegal) disposal of metallurgical slags, including blast furnace slag (BFS), steel slag (SS), stainless-slag (SSS), electric furnace ferronickel slag (EFFS) and copper slag (CS) occupies land and may release significant harmful heavy metals into the environment *via* their leaching (e.g. Deng et al., 2020; Shang et al., 2021).

In particular, the copper production chain has expanded over the last four decades, increasing environmental concerns (e.g. Corush et al., 2006; Classen et al., 2009; Gorai et al., 2003; Harish et al., 2011; Krauss et al., 1999). Thus, their safe disposal and recycling for producing goods is an alternative to uncontrolled dumping. Because of the high content of silicon dioxides, it is not possible to reuse the CS into the metallurgical cycle. For this reason, the slag are usually dumped in a specific area near the copper smelter or marketed for their single physical–mechanical characteristics (i.e. asphalt pavements (Zerazion et al., 2019). Additionally, CS are used in concretes to enhance their flexural properties or in coexistence with alloys to enhance properties such as wear resistance, hardness and mechanical performance (Brand et al., 2015; Gencel et al., 2021; Ozbay et al., 2016; Shah et al., 2021, Kumar et al., 2021 and references therein). Recently, in different studies, more industrial solid wastes such as phosphorus slag, ferronickel slag, steel slag, silicomanganese slag and copper slag are also used as alkali-activated materials (Mehdizadeh et al.2018; Wang et al., 2018; Liu et al., 2019; Nath

* Corresponding author.
E-mail address: paola.stabile@unicam.it (P. Stabile).

https://doi.org/10.1016/j.wasman.2025.115141
Received 30 April 2025; Received in revised form 1 September 2025; Accepted 18 September 2025

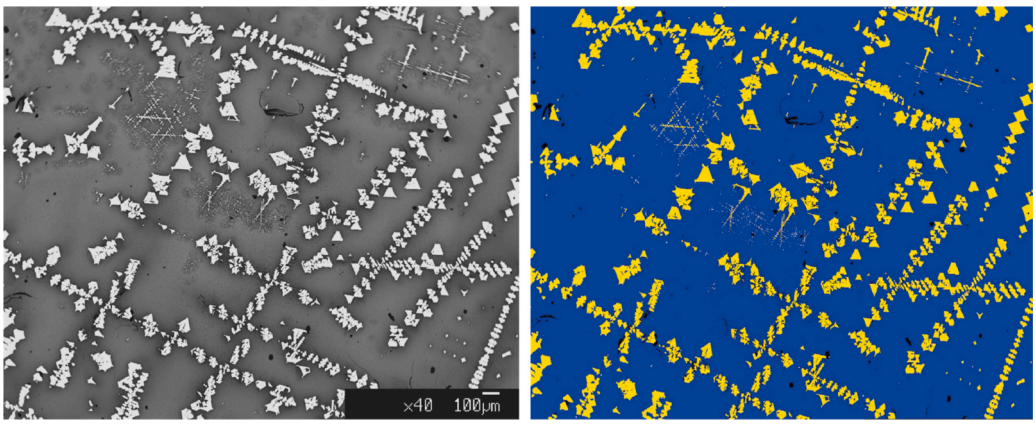

Fig. 1. Left) Representative BSE-SEM images were collected on the run-product obtained at a 10 °C/h cooling experiment; the glass is dark grey, while the crystals are white. Right) binarised images have glass reported in blue and crystals in yellow; they were used to obtain quantitative textural parameters (see text). (For interpretation of the references to colour in this figure legend, the reader is referred to the web version of this article.)

Table 1
Chemical (EPMA) and abundance (area% by image analysis on BSE-SEM micro-photographs) of phases.

	Floatglass (FG)	Copperslag (CS)	Melting starting glass	Slag-10glass	std	*Slag-10crystals	std	Slag-500glass	std	* Slag-500 crystals (NA)
area%	100	100		86.3	2.2	13.8	2.2	70.0	5.5	30 (5.5)
SiO_2	69.81	32.13	43.43	70.67	1.59	0.12	0.14	63.69	3.83	–
TiO_2	0.02	0.27	0.20							–
Al_2O_3	1.86	4.77	3.90	9.25	0.40	2.58	0.25	9.92	0.99	–
Fe_2O_3	0.42	51.42	36.12	8.25	1.61	82.67	0.71	13.02	3.94	–
ZnO	0.87	4.62	3.49	1.91	0.26	10.67	0.32	3.49	1.13	–
MgO	1.34	–	0.40	0.79	0.14	2.22	0.16	1.25	0.40	–
CaO	8.97	3.43	5.09	5.46	1.22	0.03	0.03	5.47	1.71	–
Na_2O	11.68	0.67	3.97	2.37	0.41	0.41	0.02	2.41	0.76	–
K_2O	2.06	0.66	1.08	1.04	0.11	0.02	0.02	0.82	0.24	–
BaO	1.23		0.37			0.00		0.36	0.11	–
CuO		0.81	0.57	0.51	0.11	0.74	0.16	0.55	0.22	–
P_2O_5	0.01	0.76	0.53							–
LOI	0.46		0.14							
Total	98.74	99.77	99.46	100.29				101.22		

Footnote: Data of columns float glass (FG) and copper slag (CS) are from Actalab, Material Testing Services (CA); stdv for Si, Ca and Fe oxides is $\leq$ 1.0 wt%, for Al, Mg, Na, K and Zn oxides is $\leq$ 0.5 wt%, and for all the others is 0.02 wt%. *Average chemistry of crystals analysed by EPMA for 10 and 500 °C/h cooling experiments. Crystals in the run product cooled at 500 °C/h have been considered "not analysable" (see text for further details).

and Kumar, 2017; Liu et al., 2020). At present, studies focus mainly on blast furnace (BF) slag generally rapidly cooled (quenched with water) and recycled principally as a raw material for cement manufacture or they report the effect of different minor elements (such as Ti) on slag reactiveness to be used as supplementary cementitious materials (Blotevogel et al. 2020). For instance, the effective utilization of blast furnace slag depends on its amorphous formation ability in the cooling process with phase change. Aiming at this, the crystallisation behaviour of molten blast furnace slag was observed in situ conducting isothermal and non-isothermal experiments under various cooling rate to construct the diagrams for time temperature-transformation (TTT) and continuous cooling-transformation (CCT) in the cement field (Qin et al., 2014; Lin et al., 2016).

Similarly, Pronina et al (2018) determined the cooling history of blast furnace slag (GBS) determining the TTT and CTT diagrams to better interpret the reactivity of such a product in the cementitious systems and demonstrating that the cooling rates strongly affect the energetic state of the glass, which was expressed by its fictive temperature. Further, they demonstrated the relevance of different cooling rates with regards to latent hydraulic reactivities of wet-granulated blast furnace slags (Ehrenberg et al., 2020).

Furthermore, literature has been focused on the recycling of different silica-rich solid wastes involving thermal processing to produce glassy materials or ceramics (e.g. Abudurehman et al., 2021; Bernardo et al., 2010; Binhussain et al., 2014; Deng et al., 2023; Liu et al., 2020; Shang et al., 2021; Stabile et al., 2019; Stabile et al., 2023; Stabile et al., 2025; Wu et al., 2023). The production of glass ceramics includes vitrification and crystallization processes control which directly affect also the performance of the products. Still BFS is the most common and representative slag used as a valid component for the preparation of silicate-based glass ceramics (Wu et al.2023). For example, in Wu et al. (2023), the quartz-based glasses were added to Ti-bearing BFS to prepare glass ceramics with the aim of investigating the effect of waste glass content and the temperature of treatment on the crystallization behaviour of glass-ceramics, also providing performant products in terms of flexural strength, density and chemical durability. A similar study by Deng et al. (2023) focussed on glass-ceramics prepared from ferrochromium slag and waste glass as additive, mainly evaluating the Cr-iron-leaching characteristics. Shang and co-authors (2021) presented a deep review on the preparation of metal slag –derived glass-ceramics with emphasis on the product properties. In addition to the methodology of treatment and the chemical characterization of each slag, they reported suitable nucleating agents to select to obtain glass-ceramics with selected performances (e.g. bending strength, density, etc.).

Moving from these situations on our study we explore the feasibility of combining CS and glass waste together to produce glass-ceramics without using of chemical additives. In the past, these two secondary raw materials were also used to produce homogeneous glassy materials (crystal-free); however, under certain solidification conditions, a desired content of crystals and non-crystalline phases can be grown. This

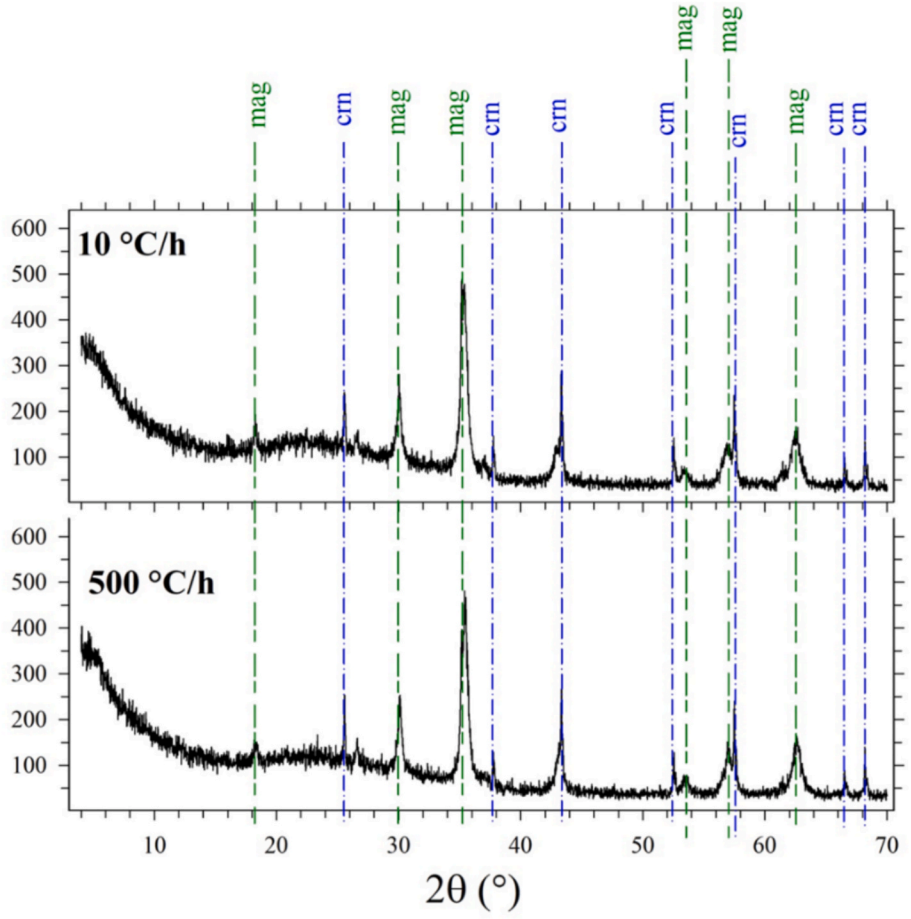

Fig. 2. XRPD spectra of the samples solidified at 10 and 500 °C/h, acquired with a X'Pert PRO from 4 to 70°, with a step scan of 8 s each 0.02° of 2θ. The most intense Bragg reflections correspond to standard crystalline phases of magnetite (mag); corundum (crn) was used as internal standard.

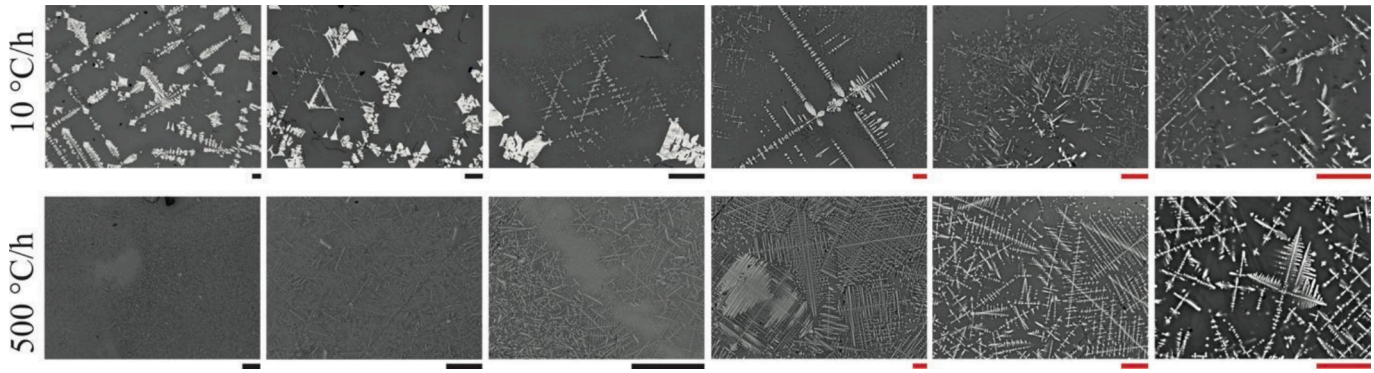

Fig. 3. BS micro photos acquired by SEM of the two run products at different magnifications (from 40 to 250x for experiments at 10 °C/h and from 200 to 1500x for the experiment at 500 °C/h); black and red bars correspond to 100 μm and 10 μm, respectively. (For interpretation of the references to colour in this figure legend, the reader is referred to the web version of this article.)

approach is relatively common in Earth Sciences domains to reproduce solidification conditions of lavas and igneous rocks (Vetere et al., 2015) and can be translated to materials sciences. The type and amount of glass and CS waste provide the bulk starting composition. At the same time, the textural and crystal-chemical attributes of phases, either crystalline or non-crystalline, are tuned by cooling conditions (cooling rate at 10 and 500 °C/h are applied) and bulk composition (Giuliani et al., 2020). Significantly, this approach does not require any nucleating agents and/or further forming other waste since the obtained recycled glass–ceramic is synthesised solely from the initial raw materials. Being the CS starting material rich of magnetic metal oxide (Fe_2O_3) in its composition, it enhances the electromagnetic sensitivity of absorbing microwaves thus providing a novel class of glass–ceramic material which have not been so fare produced for this intended purpose. Further, they represent a possible waste reduction strategy but also a valorisation of industrial waste offering a potentially more sustainable and economically competitive alternative to conventional glass–ceramic manufacturing. In contrast to state-of-the-art separate recycling, co-processing of the two waste streams offers notable benefits. Glass-ceramic formation occurs more easily, without requiring very high melting temperatures.

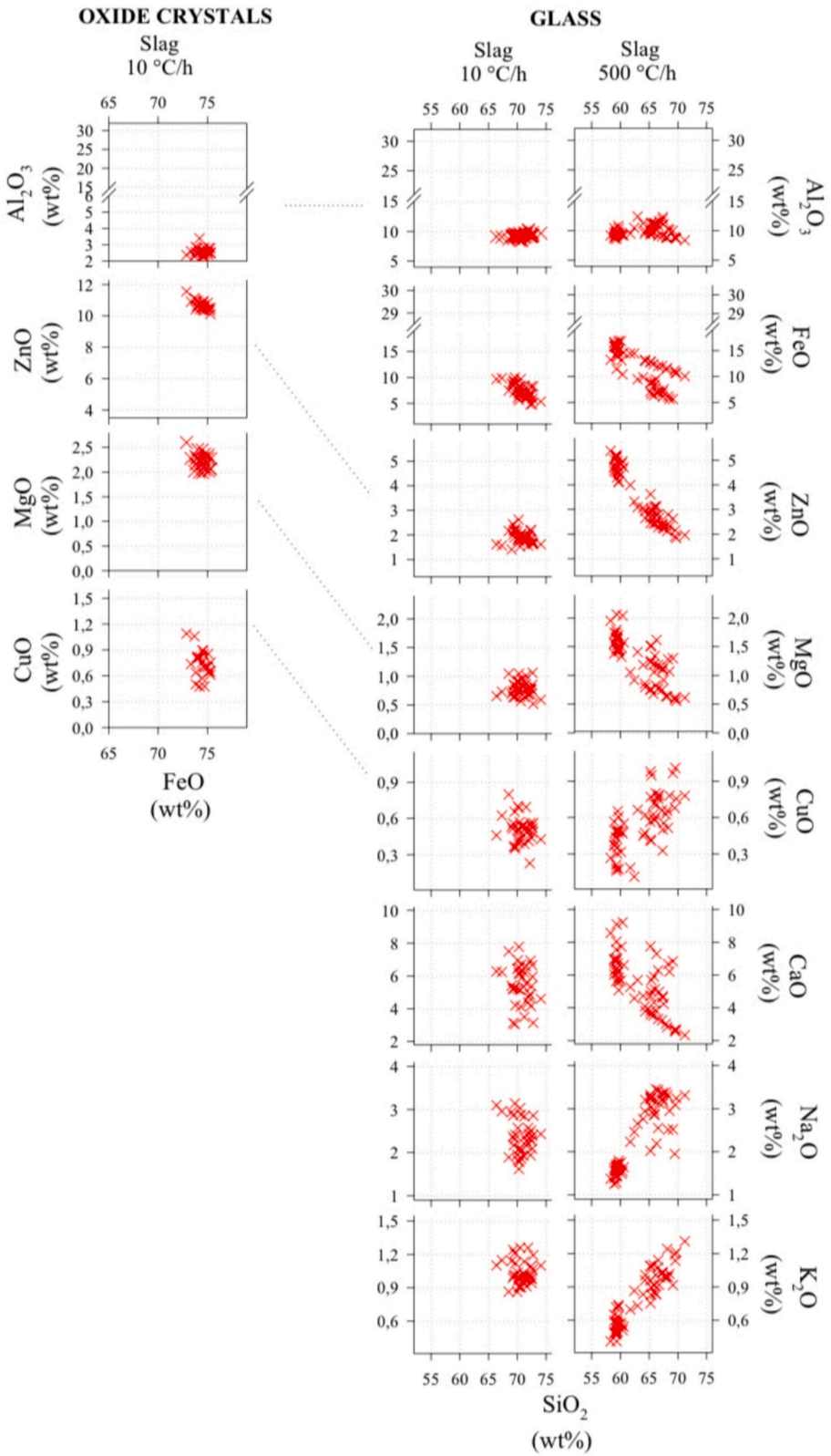

Fig. 4. Chemical variations of major oxides (wt%) in glass in both the run products, plus oxide crystals for only for the 10° C/h run-product; crystals of Slag-500 cannot be analysed with EPMA due to their tiny sizes. These data are reported in Table 1.

This means lower energy demand and reduced cost. In addition, co-processing provides: i) higher overall material recovery, ii) lower energy and cost per unit through shared heating, grinding, and refining, and iii) a smaller environmental footprint, with fewer emissions and waste streams to manage.

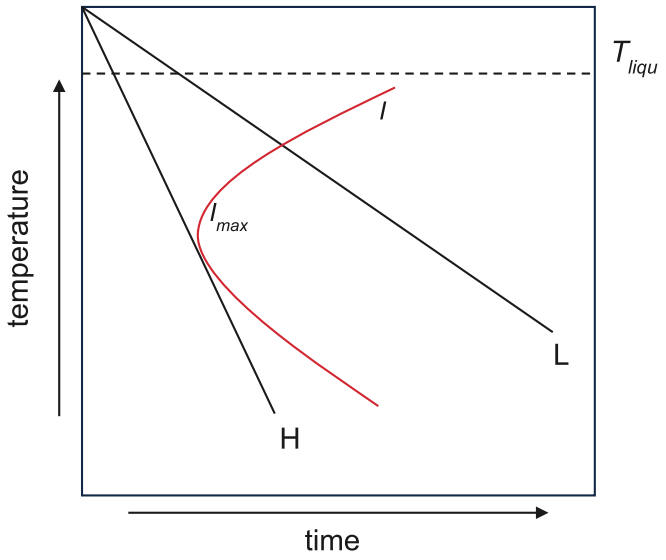

Fig. 5. Schematic temperature–time-transformation (TTT) diagram. The red curve represents the nucleation rate I, the T_{liqu} the *liquidus* temperature and the H and L black lines the intermediate (500 °C/h) and the low (10 °C/h) cooling rates; the nose or the tip of the red curve corresponds to I_{max}, *maximum* nucleation rate. (For interpretation of the references to colour in this figure legend, the reader is referred to the web version of this article.)

2. Material and methods

2.1. Starting materials, experimental and analytical procedures

FG and CS waste were considered as starting waste materials. The crushed glass was sieved to ca. 200 μm, while the provided slag had a size close to 150 μm. The slag represents the by-products of the primary copper production of Aurubis AG Company, located in Hamburg (Germany). During smelting and refining stages, a loss of material can be observed and a part of it is represented by copper slag containing different types of metals and slag-making oxides, such as iron, copper, molybdenum, arsenic, antimony, lead, precious metals, silica, alumina, calcium and magnesium oxides and sulfur (Zerazion et al., 2019). 70 wt % slag and 30 wt% of glass powders were manually mixed and placed at high temperature in a Pt crucible (3x4 cm). The crucible was gradually filled to minimise any possible pouring of the mixed material due to the trapped air in the mixed powder and/or for the very low viscosity of the liquid at high-*T*.

Five melting experiments were conducted in a Carbolite Gero TF1 16–60-180 furnace at 1550 °C for 4 h obtaining about 70 g of a homogeneous starting glass. The experiments were carried out at the experimental petrology lab at the Department of Physical Sciences, Earth and Environment of the University of Siena (Vetere et al., 2021).

To improve homogeneity, after the first 4 h, the melt was rapidly quenched on a brass plate, cooled to room temperature, crushed and subsequently re-melted. Because the strategy envisages cooling experiments, in the second melting step "2″, the Al_2O_3 crucible (1.8 cm in diameter x 2 cm height) was filled with the prepared glass powder and remelted for 4 h at 1550 °C. Finally, the produced melts were directly used as starting material for the cooling experiments. Due to the relatively large tube furnace (10 cm in diameter), some possible temperature fluctuations due to convection were expected. Thus, two ceramic cups were placed at the top and at the bottom of the crucible to minimize this effect, and one unsheathed S-type thermocouple was placed close to the crucible to monitor temperature better. The thermocouple interfaces with an S-Type thermocouples reader for recording and data logging. The temperature precision was ± 1 °C. Temperature control allow direct temperature monitoring in continuum. Experiments were performed by applying two different cooling rates of 10 and 500 °C/h after a dwell time of 20 min at 1550 °C. After run, samples were directly removed from the furnace and quenched in a water bath at room temperature (Table 1 in Supplementary Material).

After each experiment, the crucibles were cut in half and run-products extracted for X-ray diffractometer (XRPD), Microprobe (EPMA), Scanning Electron Microscopy (SEM). XRPD analyses were acquired at the Department of Engineering Enzo Ferrari (University of Modena and Reggio Emilia) using a X'Pert PRO from 4 to 70°, with a step scan of 8 s each 0.02° of 2θ. The most intense Bragg reflections have been assigned to standard crystalline phases of magnetite (mag); corundum (crn) was used as a standard.

Analyses on the FG and CS used for the cooling experiments were determined by the Actalab Material Testing Services (Ontario, CA). EPMA analyses were conducted to investigate the two cooling experiments of slag 10 and 500 °C/h, respectively. We used a Jeol-JXA8200 EDS-WDS combined (five spectrometers with twelve crystals), using 15 kV, 7.5 mA, and an electronic beam of 2.5 μm at the HTHP lab INGV of Roma. Analyses have been collected for an average of 15 crystals. Crystals in the run product cooled at 500 °C/h are small and numerous dendrites. During the analysis, the smallest size of the electron beam (2.5 μm) involves also the glass around and below the crystals, so they have been considered "not analysable" (see Fig. 1).

About 50 BSEs different magnifications (from 40 to 250x for experiments at 10 °C/h, and from 200 to 1500x for the experiment at 500 °C/h) were collected also at the INGV of Roma, by using a field-emission scanning electron microscopy (FE-SEM, JEOL 6500F) equipped with an energy-dispersive X-ray (EDX) microanalysis system.

Image analysis was performed on about 20 selected BSE microphotographs using the Image-ProPlus software http://www.mediacy.com/imageproplus). These images were selected from different regions of the sample to ensure the representativeness of the measurements, including possible microstructural heterogeneity. Each BSE-SEM microphotograph was first digitalised and calibrated, without filters or stereological correction. Crystalline and glassy phases were segmented as a function of their grey level range and then binarised with different false colors. The phase fractions were then calculated as the mean area fraction (area %). Since the phases are randomly distributed and the microstructure is isotropic at the scale of observation, the area fraction can be considered as a good approximation of the volume fraction, according to stereological principles (Higgins (2006). An example of image treatment is reported in Fig. 1. Following Higgins (2006) and Iezzi et al. (2011), each crystal is geometrically described by a best-fitting equal-area ellipse. Dendritic phases were considered individual crystals (Hammer et al., 2010; Shea and Hammer, 2013). Touching crystals and dendrites with different orientations were manually identified and separated. Chemical results referring to the glass and crystal phases are reported in Table 1.

Finally, the room temperature dielectric properties of the bulk specimen (cooled at room temperature) were measured up to the frequency of 3 GHz by means of the open-ended coaxial probe method employing an Agilent 85070E kit connected to a vector network analyzer (HP 8753C).

3. Results and discussion

Starting materials and cooling experiments chemical analyses are reported in Table 1. The two run-products solidified in both cooling experiments, Slag-10 and Slag-500, consist of spinel crystals embedded in a non-crystalline glass matrix, as straightforwardly demonstrated by both XRPD (Fig. 2) and SEM (Figs. 1 and 3) outcomes. Hot Stage Microscopy (HSM) on the starting glass was performed on the quench Slag to determine: $T_{melting}$, $T_{sintering}$ and T_g. Measured data correspond to 1447, 1152 and ~ 1000 °C, respectively.

The data support the choice of 1550 °C as the appropriate temperature for mixture homogenisation and glass preparation. This

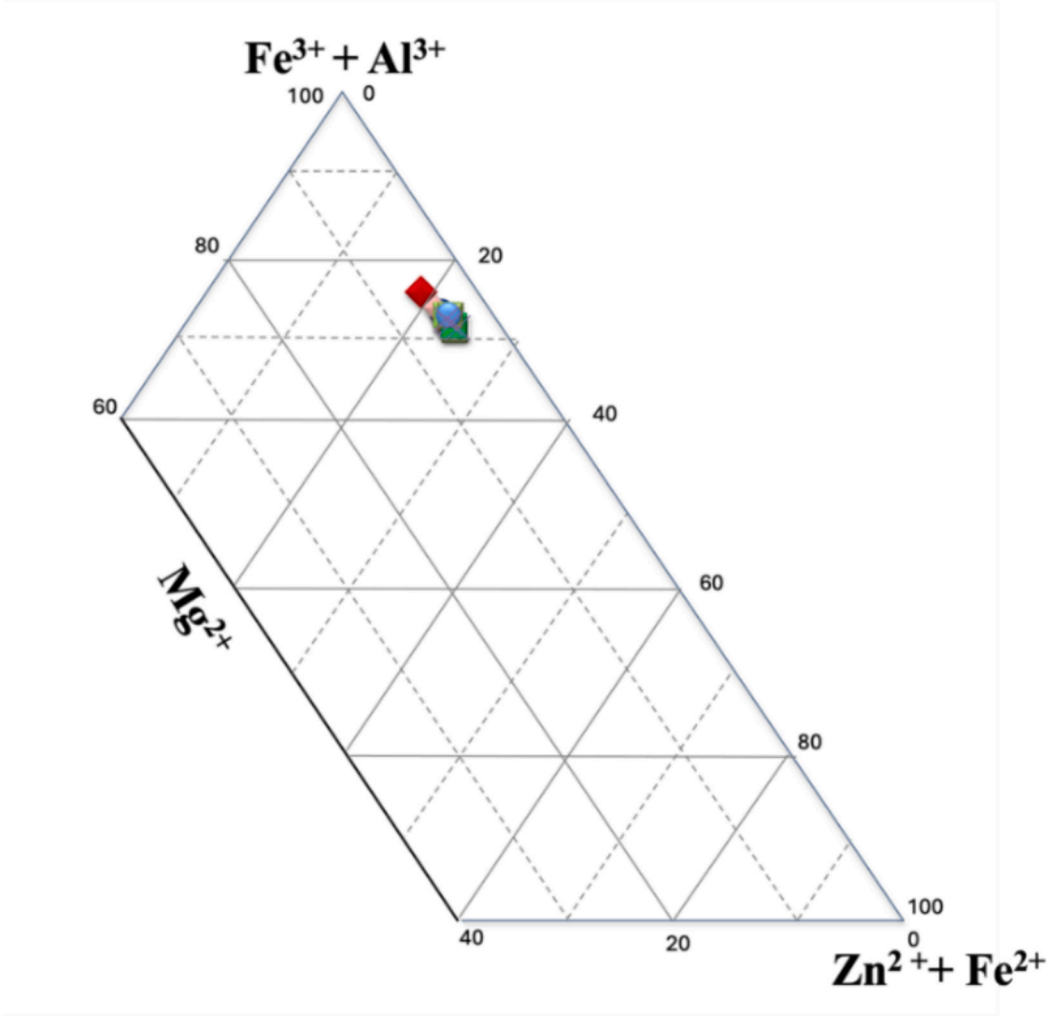

Fig. 6. Calculated apfu of Zn^{2+}, Fe^{2+}, Mg^{2+}, Fe^{3+} and Al^{3+} in spinel crystallised at 10 °C/h.

observation agrees with previous studies involving similar materials and comparable thermal paths (e.g. Shelby, 2005).

The crystal-chemical features of solidified glasses and spinel only at 10 °C/h are reported in Table 1 and displayed in Fig. 4. At 10 °C/h cooling rate, spinel is significantly enriched in Fe, Al, Mg and Zn oxides (Table 1, Fig. 4), instead, albeit abundant, spinels grown at 500 °C/h have very tiny sizes to be appropriately analysed by EPMA.

The Al_2O_3 content is higher in these samples compared to the FG and CS starting materials (Table 1), suggesting a partial dissolution and/or reaction with the alumina crucible probably due to the long dwell time at 1550 °C prior to cooling; the contamination is more significative in the portion of the run products closer to the Al_2O_3 walls of crucible and became as slower as moving towards the inner most proportion.

The oxides of the residual glass at 500 °C/h are more scattered than at 10 °C/h (Fig. 4). The residual glass at 10 °C/h is more depleted in FeO^{tot}, Al_2O_3 and MgO wt.% than its counterpart at 500 °C/h (Fig. 4).

Image analysis unveils that crystal content, i.e. spinel amount, shifts from 13.8 to 30 area % as cooling rate moves from 10 to 500 °C/h (Table 1), with larger crystal size at lower cooling rate (Fig. 3). This unexpected trend can be explained by a schematic time–temperature-transformation (TTT) diagram (Fig. 5). For instance, we can employ the TTT curves to distinguish and interpret the two general cases of high (H) and low (L) cooling rates in Fig. 5, which correspond to our scenario of 500 and 10 °C/h cooling rates, respectively. The nucleation rate is maximised at I_{max} and the induction time for the onset of nucleation, τ_{min} is the lowest one (Fokin et al., 2003; Lasaga, 1997; Roskosz et al., 2005). Such a situation corresponds to the nose or the tipping point of the TTT curve; moving above or below I_{max} or τ_{min}, the nucleation rate I decreases and the induction time τ increases (Fig. 5; Fokin et al., 2003; Iezzi et al., 2009; Vetere et al., 2013). Since the run-product Slag-500 is composed of many tiny-sized spinels and the cooling rate is high (500 °C/h), such a situation is captured by the line H; conversely, the relatively few and large spinels at 10 °C/h reappraise the intersection of the red I curve for L (Fig. 5). After the first pulse of nucleation represented by the relatively few and large-sized spinel at 10 °C/h and by the numerous and tiny-sized spinels at 500 °C/h, the residual melt becomes enriched in SiO_2 and depleted in all the other oxides (Table 1), reducing further crystallization (Fig. 3). At the same time, the high SiO_2 content enhances the glass-forming ability (GFA) making the melt reluctant to nucleate (Vetere et al., 2015).

According to electric charge neutrality (also involving ferric and ferrous speciation) per four oxygens and three cations, plus crystallographic constraints (Gennaro et al., 2024; Stormer 1983), the apfu (atom per formula unit) of spinel at 10 °C/h corresponds to a Zn, Al, Mg-bearing magnetite (Fig. 6). Specifically, since the $\Sigma R^{3+}/R^{2+}$ ratio is from 2 and 3, the spinel crystallised at 10 °C/h belong to the 2–3 spinel subgroup ($A^{2+}B^{3+}O_4$), with Fe^{3+} (plus Al^{3+}) as the predominant B-cation, whereas the dominant A-cations are Fe^{2+}, Mg^{2+} and Zn^{2+} (Bosi et al., 2019). Spinel chemistry reflects the cooling rate conditions, emphasising the distribution of Fe and Zn oxides between crystals and residual glasses. Only at 10 °C/h the crystals of spinels can be directly measured (Table 1), which is compatible with Fe_2O_3, ZnO, MgO and

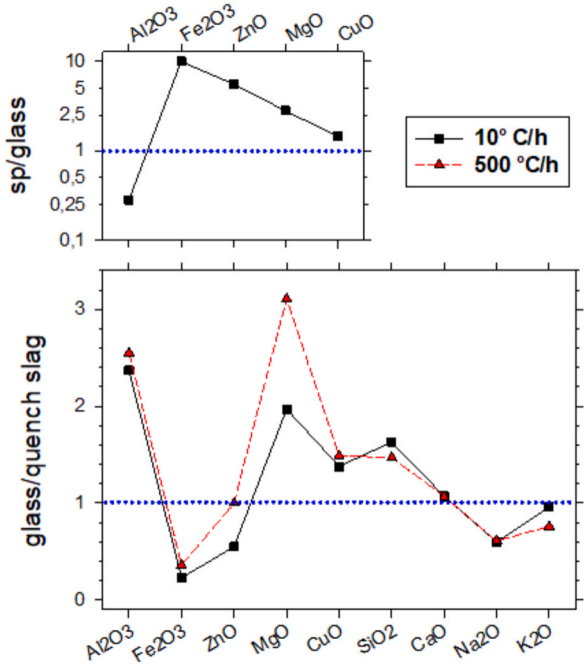

Fig. 7. (top) Ratios of oxides in crystals of spinel *vs* residual glass at 10 °C/h and (bottom) glasses at 10 and 500 °C/h *vs* quenched glass (bulk chemical composition).

CuO (in order of compatibility) and incompatible with Al_2O_3 (Fig. 7). This is corroborated by the incompatibility of Fe_2O_3 and ZnO in the residual glass at 10 °C/h (Fig. 7). By contrast MgO and CuO are compatible in spinel/glass and glass/quench_glass at 10 °C/h; these discrepancies can be ascribed to the low amounts of MgO and CuO measured in the quench glass and residual glass (Table 1). At 500 °C/h, the only available distribution can be inferred from the ratio between oxides in the residual glass *vs* the quenched glass, which indirectly testifies that only Fe_2O_3 is highly incorporated in the tiny spinels. In contrast, Zn is less compatible than at 10 °C/h (Fig. 7).

A final aspect driven by the different rates of cooling concerns the crystal size and growth rate of spinels. For the sake of simplicity, it is possible to crudely assume that at 10 and 500 °C/h the sizes of spinel are on the order of 20 to 200 μm (Fig. 3). Then, it is plausible to assume a putative temperature for the crystallisation of spinel comprised between 1300 down to 1000 °C; this thermal range is simplified but qualitatively reliable considering the bulk composition of this system and relatively close magmatic systems. In turn, the thermal range is 300 °C, which is experienced for 0.6 and 30 h in the rapid and sluggish cooling experiments. These assumptions unveil that at 10 and 500 °C/h the crystal growth rate of spinel could be on the order of $1{,}8{\cdot}10^{-8}$ cm/s and $9.3{\cdot}10^{-6}$ cm/s, respectively. Indeed, the thermal range for the growth of spinel must be more restricted than at 10 °C/h according to the TTT diagram (Fig. 5). In turn, the spinel growth at 500 °C/h should be crystallised with a growth rate even larger than $9.3{\cdot}10^{-6}$ cm/s. The increasing growth rate of spinels with the increase of the cooling rates is in line with previous studies on chemically complex silicate systems (Gennaro et al., 2024; Giuliani et al., 2020, 2022). Moreover, even assuming a lower thermal range of 150 °C, the resulting growth rate would have been 3.70·10-8 and 1.85·10-5 cm/s for 10 and 500 °C/h, respectively.

3.1. *Implications of the study for industrial applications*

The use of copper slag in the glass–ceramic production enhances the microwave absorption performance of the product. This has been evaluated by performing microwave heating tests and the results are reported in Fig. 8, where the measured ε' (stored energy) and ε'' (dissipated energy) are plotted as a function of frequency, together with the corresponding values of the dielectric loss factor tan δ (tan δ = ε'' / ε').

This parameter provides insight into the material's ability to absorb electromagnetic energy and convert it into heat. In particular, the value of tan δ at 2.45 GHz was evaluated, as this is the most widely used frequency among those authorized and allocated for industrial, scientific or medical applications, and it can be freely used worldwide. The bulk sample exhibits a tan δ of 0.23 at 2.45 GHz, which is higher than that of water (0.15) and close to that of Silicon-carbide (SiC) tile (0.37) (Zerazion et al., 2019; Hu et al., 2022). This makes these new products

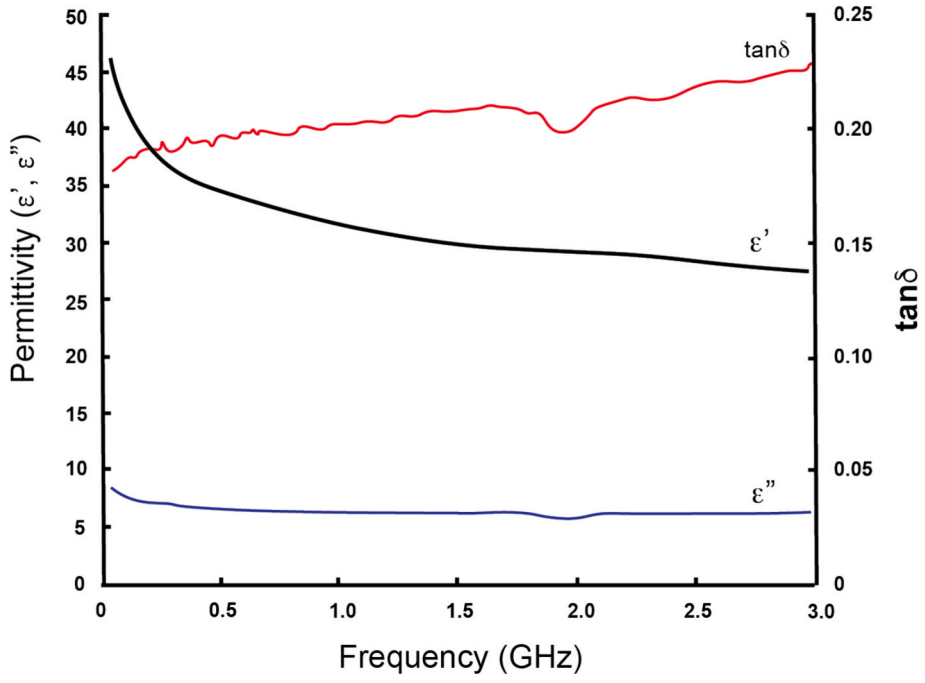

Fig. 8. Room temperature dielectric properties of the bulk specimen as a function of frequency.

promising for industrial applications in the glass–ceramic manufacturing as potential microwave absorbers.

Moreover, besides the valorisation of industrial waste, our process offers a potentially more sustainable and economically competitive alternative to traditional glass–ceramic manufacturing.

The energy footprint (E) for the reaching of the melting temperature of the mixture has been estimated at approximately 1602 kJ/kg, based on the standard energy balance equation below

$$E(J) = mxcpx\Delta T \quad (1)$$

where m is the sample mass (kg), cp is the specific Heat (J/Kg* °C), ΔT is the temperature variation (°C). The energy of fusion must be also accounted, and we calculated it assuming a glass of basaltic composition treated a T of 1000 °C. Thus, using the cp values found in literature (Navrotsky et al., 1989; Lesher and Spera, 2015; Ye et al., 2023), we estimated the total E of fusion of ca.1337 kJ. The overall energy consumption or energy footprint results lower than 3000 kJ. Considering that the energy footprint of conventional glass-ceramics is complex to estimate due to its dependence on several factors—such as (i) the specific manufacturing process, (ii) the type of glass–ceramic, and (iii) the energy source used—it's important to note that the potential energy demand for glass production is approximately 5000 kJ. This demand is even higher in glass–ceramic production because of additional energy-intensive processes, such as spray drying, among others. Additionally, a similar study on the production of glass-ceramics from MSW fly ash reports an energy demand of around 9,000 kJ per kilogram of product (Barracco et al., 2023). Therefore, the choice and use of these secondary raw materials, i.e. copper slag (70 %) and float glass cullet (30 %), can significantly reduce material and environmental costs.

4. Conclusions

An alternative way to produce new glass ceramics, from two broadly available waste materials is reported without using additives, solutions or fluxing agents. The waste materials must be mixed and then melted to obtain a homogeneous liquid. Controlled cooling rates must be applied to this liquid, with a bulk composition containing SiO_2 similar to magmatic rocks (here 10 and 500 °C/h) to concentrate several elements in a phase. Lower cooling rates allow high Fe and Zn incorporation in the spinel structure, the unique solidified crystalline phase, and slow down their growth. By contrast, higher kinetics conditions cause the rapid crystallisation of more numerous and smaller spinel crystals. Also, at higher cooling rate of 500 °C/h, we can infer a less compatibility (and minor incorporation) of Zn in the spinel phase only if consider the resulting residual glass composition, but still potentially concentrating Fe in the crystal structure. In light of this, the amount and the chemical composition of spinel crystals can be modulated by adjusting the cooling rate.

The resulting glass-ceramics, obtained from waste materials, can then be used for direct applications or crushed to separate spinel crystals from silicate glass easily. This process can be implemented for dedicated industrial applications (see Sharma et al., 2024; Zerazion et al., 2019), such as the design of glass-ceramics with desired macroscopic features (optical, electronic, magnetic, etc.) or to concentrate certain elements in easily separable phases after crushing, avoiding wet chemical treatments and decreasing the environmental impact. For safety, if these materials also solidify potentially harmful metals in the glass matrix and as nuclei to induce crystallization during the thermal treatment, a further study will include the metal leaching issue to examine the potential release of substances from the educts and products of the presented methodological approach.

CRediT authorship contribution statement

Paola Stabile: Writing – original draft, Visualization, Validation, Investigation, Data curation. **Francesco Vetere:** Writing – review & editing, Writing – original draft, Resources, Methodology, Investigation, Data curation, Conceptualization. **Letizia Giuliani:** Methodology, Investigation, Data curation. **Cristina Siligardi:** Methodology, Investigation, Data curation. **Consuelo Mugoni:** Methodology, Investigation, Data curation. **Manuela Nazzari:** Resources, Investigation, Data curation. **Gianluca Iezzi:** Writing – review & editing, Writing – original draft, Validation, Methodology, Investigation, Funding acquisition, Data curation, Conceptualization.

Funding

This study was supported by the i) PRIN (2009PZ47NA_003) project "Time Scales of Solidification in Magmas: Application to Volcanic Eruptions, Silicate Melts, Glasses, Glass-Ceramics", ii) project "UP-CDW: Riuso upcycling dei Construction Demolition Waste (CDW)" financed by the PNC Mis B4.1 Centri di Ricerca per l'Innovazione nelle Aree del Sisma 2009–2016 (PRJ-0362), iii) PRIN2022 of MUR "RUB2RES: Rubble-to-Resource Earth science knowledge for sorting and recycling Construction and Demolition Waste" (D53D23004510006), iv) by the "Fondi Ateneo of the University G. D'Annunzio" awarded and assigned to **Iezzi G.** The "Piano di Sostegno alla Ricerca 2022 per finanziamenti a progetti di ricerca Curiosity-driven (F-CUR CREAMI)" awarded to **Vetere F.** is also acknowledged.

Declaration of competing interest

The authors declare the following financial interests/personal relationships which may be considered as potential competing interests: Gianluca Iezzi reports financial support was provided by Gabriele d'Annunzio University of Chieti and Pescara. Francesco Vetere reports financial support was provided by University of Siena Department of Physics Earth and Environmental Sciences. If there are other authors, they declare that they have no known competing financial interests or personal relationships that could have appeared to influence the work reported in this paper.

Appendix A. Supplementary data

Supplementary data to this article can be found online at https://doi.org/10.1016/j.wasman.2025.115141.

Data availability

No data was used for the research described in the article.

References

Abudurehman, A., Stabile, P., Carroll, M.R., Santulli, C., Paris, E., 2021. Mineralogical and chemical characterisation of CDW as function of particle size and thermal treatments for potential recycling. Detritus 15, 40–50.

Barracco, F., Demichelis, F., Sharifikolouei, E., Ferraris, M., Fino, D., Tommasi, T., 2023. Life cycle assessment for the production of MSWI fly-ash based porous glass-ceramics: Scenarios based on the contribution of silica sources, methane aided, and energy recoveries, Waste Manage., 157, 301–311, ISSN 0956-053X.

Bernardo, E., Bonomo, A.D., 2010. Optimisation of sintered glass–ceramics from an industrial waste glass. Ceram. Int. 36(5), 1675–1680. https://doi.org/10.1016/j.ceramint.2010.02.047. ISSN 0272-8842.

Binhussain, M.A., Marangoni, M., Bernardo, E., Colombo, P., 2014. Sintered and glazed glass-ceramics from natural and waste raw materials. Ceram. Int. 40(2), 3543–3551. https://doi.org/10.1016/j.ceramint.2013.09.074. ISSN 0272-8842.

Blotevogel, S., Steger, L., Hart, D., Doussang, L., Kaknics, J., et al., 2020. Effect of TiO2 and 11 minor elements on the reactivity of ground-granulated blast-furnace slag in blended cements. J. Am. Ceram. Soc. https://doi.org/10.1111/jace.17431ff. ffhal-02931126f.

Bosi, F., Biagioni, C., Pasero, M., 2019. Nomenclature and classification of the spinel supergroup. Eur. J. Mineral. 183–192.

Brand, A.S., Roesler, J.R., 2015. Steel furnace slag aggregate expansion and hardened concrete properties. Cem. Concr. Comp. 60, 1–9. https://doi.org/10.1016/j.cemconcomp.2015.04.006.

Classen, M., Althaus, H.J., Blaser, S., Tuchschmid, M., Jungbluth, N., Doka, G., Faist Emmenegger, M., Scharnhorst, W., 2009. Life Cycle Inventories of Metals. Final report Ecoinvent data v2. 1, No 10. EMPA, Swiss Centre for Life Cycle Inventories, Dübendorf, CH. http://www.ecoinvent.org/.

Coetzee, J., Bansal, N., Chirwa, E.M.N., 2020. Chromium in environment, its toxic effect from chromite-mining and ferrochrome industries, and its possible bioremediation. Expos. Health 12 (1), 51–62. https://doi.org/10.1007/s12403-018- 0284-z. Springer.

Corush, S., Ergun, O.N., Cheng, T.W., 2006. Treatment of copper industry waste and production of sintered glass–ceramic. Waste Manag. Res. 24, 234–241. http://journals.sagepub.com/doi/abs/10.1177/0734242X06062600.

Deng, L., Yun, F., Jia, R., Li, H., Jia, X., Shi, Y., Zhang, X., 2020. Effect of SiO2/MgO ratio on the crystallization behavior, structure, and properties of wollastonite-augite glass-ceramics derived from stainless-steel slag. Mater. Chem. Phys. 239, 122039. https://doi.org/10.1016/j.matchemphys.2019.122039.

Deng, S., Li, C., Guo, H., Zhao, W., Yan, B., Li, P., 2023. Crystallization characteristics, microstructural evolution, and Cr migration mechanism of glass-ceramics synthesized entirely from low-carbon ferrochromium slag and waste glass. J. Hazard. Mater. 445. https://doi.org/10.1016/j.jhazmat.2022.130621, 130621, ISSN 0304-3894.

Dino, G.A., Cavallo, A., Rossetti, P., Garamvolgyi, E., Sandor, R., Coulon, F., 2020. Towards sustainable mining: exploiting raw materials from extractive waste facilities. Sustainability 12 (6).

Ehrenberg, A., Romero Sarcos, N., Hart, D., et al., 2020. Influence of the thermal history of granulated blast furnace slags on their latent hydraulic reactivity in cementitious systems. J. Sustain. Metall. 6, 207–215. https://doi.org/10.1007/s40831-020-00269-4.

Fokin, V.M., Zanotto, E.D., Schmelzer, J.W.P., 2003. Homogeneous nucleation versus glass transition temperature of silicate glasses. J. Non Cryst. Solids 321, 52–65.

Gennaro, E., Iezzi, G., Nazzari, M., Vetere, F., Scarlato, P., Giuliani, L., Zellmer, G., 2024. The kinetic effect induced by variable cooling rate on the crystal-chemistry of spinel in basaltic systems revealed by EPMA mapping. Am. Mineral. 109, 1171–1180. https://doi.org/10.2138/am-2023-9014.

Gencel, O., Karadag, O., Oren, O.H., Bilir, T., 2021. Steel slag and its applications in cement and concrete technology: a review. Constr. Build. Mater. 283, 122783. https://doi.org/10.1016/j.conbuildmat.2021.122783.

Giuliani, L., Iezzi, G., Vetere, F., Behrens, H., Mollo, S., Cauti, F., Ventura, G., Scarlato, P., 2020. Evolution of textures, crystal size distributions and growth rates of plagioclase, clinopyroxene and spinel crystallized at variable cooling rates from a mid-ocean ridge basaltic melt. Earth Sci. Rev. 204, 103165. https://doi.org/10.1016/j.earscirev.2020.103165.

Giuliani, L., Vetere, F., Iezzi, G., Nazzari, M., Mollo, S., Behrens, H., Scarlato, P., Ventura, G., 2022. Crystal-chemical variations of spinel, clinopyroxene, and plagioclase in MORB basaltic melt induced by continuous cooling, 120765, ISSN 0009-2541 Chem. Geol. 594. https://doi.org/10.1016/j.chemgeo.2022.120765.

Gorai, B., Jana, R.K., 2003. Characteristics and utilisation of cop- per slag—a review. Resour. Conserv. Recycl. **39**(4), 299–313. http://www.sciencedirect.com/science/article/pii/ S0921344902001714.

Hammer, J.E., Sharp, T.G., Wessel, P., 2010. Heterogeneous nucleation and apitaxial crystal growth of magmatic minerals. Geology 4, 367–370. https://doi.org/10.1130/G30601.1.

Harish, V., Sreepada, R. A., Suryavanshi, U., Shanmuganathan, P., Sumathy, A., 2011. Assessing the effect of leachate of copper slag from the ISASMELT process on cell growth and proximate components in microalgae, *Chlorella vulgaris* (Beijerinck). Toxicol. Environ. Chem. 93(7), 1399–1412. http://www.tandfonline.com/doi/ full/10.1080/02772248.2011.588393.

Higgins, M.D., 2006. Quantitative Textural Measurement in Igneous and Metamorphic Petrology. Cambridge University Press, Cambridge.

Hu, C., Li, P., Zhu, Y., Zhao, Q., Zhang, H., 2022. Experimental study on microwave absorption properties of HMA containing copper slag, 127850, ISSN 0950-0618 Constr. Build. Mater. 341. https://doi.org/10.1016/j.conbuildmat.2022.127850.

Iezzi, G., Mollo, S., Ventura, G., 2009. Solidification behaviour of natural silicate melts and volcanological implications. In: Lewis, N., Moretti, A. (Eds.), Volcanoes: Formation, Eruptions and Modelling. Nova Publishers, New York, pp. 127–151.

Iezzi, G., Mollo, S., Torresi, G., Ventura, G., Cavallo, A., Scarlato, P., 2011. Experimental solidification of an andesitic melt by cooling. Chem. Geol. 283, 261–273. https://doi.org/10.1016/j.chemgeo.2011.01.024.

Krauss, U., Wagner, H., Mori, G., 199. Stoffmengenflüsse und Ener- giebedarf bei der Gewinnung ausgewählter mineralischer Rohst- offe. In: Teilstudie Kupfer. Geologisches Jahrbuch, Vol. Sonder- hefte SH 9. Bundesanstalt für Geowissenschaften und Rohstoffe, Hannover.

Kumar, M.H., Mohanta, N.R., Samantaray, S., et al., 2021. Combined effect of waste glass powder and recycled steel fibers on mechanical behavior of concrete. SN Appl. Sci. 3, 350. https://doi.org/10.1007/s42452-021-04353-6.

Kurtulus, C., Kurtulus, R., Kavas, T., 2021. Foam glass derived from ferrochrome slag and waste container glass: Synthesis and extensive characterizations. Ceram. Int. 47 (2021), 24997–25008.

Lasaga, A.C., 1997. Kinetic Theory in the Earth Sciences. Princeton Unveristy Press, Princeton, NY, USA.

Lesher, L.E., Spera, J.F., 2015. Chapter 5 - Thermodynamic and Transport Properties of Silicate Melts and Magma, Editor(s): Haraldur Sigurdsson, The Encyclopedia of Volcanoes (Second Edition), Academic Press, Pages 113-141, ISBN 9780123859389, DOI: 10.1016/B978-0-12-385938-9.00005-5.

Lin, B., Wang, H., Zhu, X., Liao, Q., Ding, B., 2016. Crystallization properties of molten blast furnace slag at different cooling rates. Appl. Therm. Eng. 96, 432–440. https://doi.org/10.1016/j.applthermaleng.2015.11.075. ISSN 1359-4311.

Liu, Z., Zhang, D., Li, L., Wang, J., Shao, N., Wang, D., 2019. Microstructure and phase evolution of alkali-activated steel slag during early age. Constr. Build. Mater. 204, 158–165.

Liu, L., Yu, H., Li, Y., Zhang, Z., 2020. Stabilization behavior and mechanism of heavy metals in eco-friendly glass-ceramics derived from wastes. J. Clean. Prod. 269, 122417. https://doi.org/10.1016/j.jclepro.2020.122417.

Mehdizadeh, H., Kani, E.N., Sanchez, A.P., Fernandez-Jimenez, A., 2018. Rheology of activated phosphorus slag with lime and alkaline salts. Cem. Concr. Res. 113, 121–129.

Nath, S.K., Kumar, S., 2017. Reaction kinetics, microstructure and strength behavior of alkali activated silico-manganese (SiMn) slag-Fly ash blends. Constr. Build. Mater. 147, 371–379.

Navrotsky, A., Ziegle, D., Oestrike, R., Maniar, P., 1989, Calorimetry of silicate melts at 1773 K: measurement of enthalpies of fusion and of mixing in the systems diopside-anorthite-albite and anorthite-forsterite, Contrib Mineral Petrol, 101: 122-130.

Ozbay, E., Erdemir, M., Durmus, H.I., 2016. Utilization and efficiency of ground granulated blast furnace slag on concrete properties - a review. Constr. Build. Mater. 105, 423–434. https://doi.org/10.1016/j.conbuildmat.2015.12.153.

Pronina, N., Krüger, S., Bornhöft, H.J., Deubener, J., Ehrenberg, A., 2018. Cooling history of a wet-granulated blast furnace slag. J. Non Cryst. Solids 499, 344–349.

Qin, Y.L., Lv, X.W., Zhang, J., Hao, J.L., Bai, C.G., 2015. Determination of optimum blast furnace slag cooling rate for slag recycling in cement manufacture. Ironmaking Steelmaking 42 (5), 395–400.

Ramteke, D.D., et al., 2021. Up-cycling of 'unrecyclable' glasses in glass-based foams by weak alkali-activation, gel casting and low-temperature sintering. J. Clean. Prod. 278. https://doi.org/10.1016/j.jclepro.2020.123985.

Roskosz, M., Toplis, M.J., Besson, P., Richet, P., 2005. Nucleation mechanisms: a crystal chemical investigation of phases forming in highly supercooled aluminosilicate liquids. J. Non Cryst. Solids 351, 1266–1282.

Shah, S.N., Mo, K.H., Yap, S.P., Yang, J., Ling, T.C., 2021. Lightweight foamed concrete as a promising avenue for incorporating waste materials: a review," *Resources*. Conserv. Recycl. 164. https://doi.org/10.1016/j.resconrec.2020.105103. Elsevier B. V.

Shang, W., Peng, Z., Huang, Y., Gu, F., Zhang, J., Tang, H., Yang, L., Tian, W., Rao, M., Li, G., Jiang, T., 2021. Production of glass-ceramics from metallurgical slags. J. Cleaner Prod. 317. https://doi.org/10.1016/j.jclepro.2021.128220. ISSN 0959-6526, 128220.

Sharma, S., Parne, S.R., Panda, S.S.S., Gandi, S., 2024. Progress in microwave absorbing materials: A critical review. Adv. Colloid Interface Sci. 327. https://doi.org/10.1016/j.cis.2024.103143. ISSN 0001-8686, 103143.

Shea, T., Hammer, J.E., 2013. Kinetics of cooling- and decompression-induced crystallization in hydrous mafic-intermediate magmas. J. Vocanol. Geotherm. Res. 260, 127–145. https://doi.org/10.1016/j.jvolgeores.2013.04.018.

Shelby, J.E., 2005. Introduction to Glass Science and Technology, 2nd edition. Padstow, Conwall, UK.

Spooren, J., et al., 2020. Near-zero-waste processing of low-grade, complex primary ores and secondary raw materials in Europe: technology development trends. Resour. Conserv. Recycl. 160, 104919. https://doi.org/10.1016/j. resconrec.2020.104919.

Stabile, P., Bello, M., Petrelli, M., Paris, E., Carroll, M.R., 2019. Vitrification treatment of municipal solid waste bottom ash. Waste Manag. 95, 250–258.

Stabile, P., Abudurahman, A., Carroll, M.R., Paris, E., 2023. Bulk composition effects on vitrification of mixed fine construction– demolition and inorganic solid waste. Minerals 13, 1378. https://doi.org/10.3390/min13111378.

Stabile, P., Fornasini, L., Pasetti, L., et al., 2025. Characterization of mixed- waste glasses in the CAS system: insights from differential scanning calorimetry and Raman spectroscopy. Eur. Phys. J. plus 140, 739. https://doi.org/10.1140/epjp/s13360-025-06677-3.

Stormer Jr., J.C., 1983. The effects of recalculation on estimates of temperature and oxygen fugacity from analyses of multicomponent iron-titanium oxides. Am. Mineral. 68, 586–594.

Vetere, F., Iezzi, G., Beherens, H., Cavallo, A., Misiti, V., Dietrich, M., Knipping, J., Ventura, G., Mollo, S., 2013. Intrinsic solidification behaviour of basaltic to rhyolitic melts: a cooling rate experimental study. Chem. Geol. 354, 233–242.

Vetere, F., Iezzi, G., Behrens, H., Holtz, F., Ventura, G., Misiti, V., Cavallo, A., Mollo, S., Dietrich, M., 2015. Glass forming ability and crystallisation behaviour of sub-alkaline silicate melts. Earth-Sci. Rev. 150, 25–44. https://doi.org/10.1016/j.earscirev.2015.07.001. ISSN 0012-8252.

Vetere, F., Petrelli, M., Perugini, D., Haselbach, S., Morgavi, D., Pisello, A., Iezzi, G., Holtz, F., 2021. Rheological evolution of eruptible basaltic-andesite magmas under dynamic conditions: The importance of plagioclase growth rates. J. Volcanol. Geotherm. Res. 420. https://doi.org/10.1016/j.jvolgeores.2021.107411, 107411, ISSN 0377-0273.

Wang, D., Wang, Q., Zhuang, S., Yang, J., 2018. Evaluation of alkali-activated blast furnace ferronickel slag as a cementitious material: Reaction mechanism, engineering properties and leaching behaviors. Constr. Build. Mater. 188, 860–873.

Wu, F., Hu, P., Hu, F., Tian, Z., Tang, J., Zhang, P., et al., 2023. Multifunctional MXene/C aerogels for enhanced microwave absorption and thermal insulation. Nano-Micro Lett; 15:194.

Ye, C., Zhang, M., Yang, S., Stephen, M., Huang, A., Liu, X., Zhang, X., 2023.Application of copper slags in encapsulating high-temperature phase change thermal storage

particles, Sol. Energy Mater. Sol. Cells, Vol. 254, 112257, ISSN 0927-0248, DOI: 10.1016/j.solmat.2023.112257.
Zerazion, E., Pini, M., Mugoni, C., Siligardi, C., Veronesi, P., Ferrari, A.M., 2019. E-LCA of two microwave absorbers obtained from slag of copper primary production. Waste Biomass Valor 10, 733–745. https://doi.org/10.1007/s12649-017-0081-0.
Zibret, G., et al., 2020. National mineral waste databases as an information source for assessing material recovery potential from mine waste, tailings and metallurgical waste. Minerals 10 (5). https://doi.org/10.3390/min10050446.